



Electrochemical and theoretical quantum approaches on the inhibition of mild steel corrosion in acidic medium containing chloride using synthesized 1H-indole-2,3-dione derivative

F. -Z. Qachchachi^{1,2}, Y. Kandri Rodi¹, H. Elmsellem^{3*}, A. Elyoussfi³, H. Steli⁴,
A. Haoudi², A. Mazzah⁵, Y. Ouzidan¹, N. K. Sebbar⁶, E. M. Essassi⁶

¹Laboratoire de Chimie Organique Appliquée, Université Sidi Mohamed Ben Abdallah, Faculté des Sciences et Techniques, Route d'Immouzzar, BP 2202 Fes, Morocco.

²Laboratoire de Chimie Appliquée, Université Sidi Mohamed Ben Abdallah, Faculté des Sciences et Techniques, Route d'Immouzzar, BP 2202 Fès, Morocco,

³Laboratoire de chimie analytique appliquée, matériaux et environnement (LC2AME), Faculté des Sciences, B.P. 717, 60000 Oujda, Morocco

⁴Laboratoire mécanique & énergétique, Faculté des Sciences, Université Mohammed Premier, Oujda, Maroc

⁵Laboratoire de Spectrochimie Infra-rouge et Raman UMR8516, Université des Sciences et Techniques de Lille, 59655 Villeneuve d'Ascq Cedex, France

⁶Laboratoire de Chimie Organique Hétérocyclique, URAC 21, Pôle de Compétences Pharmacochimie, Mohammed V University in Rabat, Faculté des Sciences, Av. Ibn Battouta, BP 1014 Rabat, Morocco

Received 09 Feb 2016, Revised 02 Aug 2016, Accepted 05 Aug 2016

*Corresponding author. E-mail : h.elmsellem@yahoo.fr Tél : +212670923431

Abstract

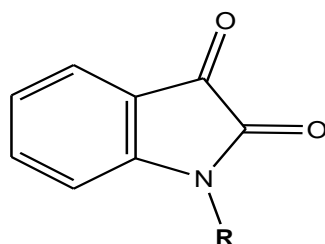
1H-Indole-2,3-dione derivatives (P2 and P3), have been synthesized characterized by NMR spectroscopy. and tested as corrosion inhibitors for mild steel in HCl solution using potentiodynamic polarization curves and electrochemical impedance spectroscopy. Potentiodynamic polarization curve measurements showed that the investigated compounds were a mixed-type inhibitors. Their inhibition efficiencies improved with concentration and reached a maximum at 10^{-3} M . Electrochemical impedance spectroscopy (EIS) studies suggested that P3 inhibit mild steel corrosion by becoming adsorbate at the metallic/electrolyte surfaces. Adsorption of the inhibitors on the mild steel surface was found to obey Langmuir's adsorption isotherm. Further, the electronic structural calculations using quantum chemical methods were found to be in a good agreement with the results of the experimental studies.

Keywords: Mild steel, 1H-indole-2,3-dione, EIS, Corrosion, Weight loss, Electrochemical, DFT.

1. Introduction

Over the years, Isatin (1H-indole-2,3-dione) derivatives are synthetically versatile substrates, where they can be used for the synthesis of a large variety of heterocyclic compounds, such as indoles and quinolines, and as raw material for drug synthesis. They were reported to possess wide spectrum of activity like antibacterial[1], antifungal[2], anticonvulsant[3], anti-HIV[4], antidepressant[5] and antiinflammatory[6] etc.,

The present study aimed to test new compounds P2 and P3 on the corrosion of mild steel in 1 M hydrochloric acid solution. They are prepared by alkylation reactions of isatin under phase-transfer catalysis conditions using tetra n-butyl ammonium bromide (TBAB) as catalyst and potassium carbonate as base (Figure 1).



P2: R= -CH₂C≡CH

P3: R=-CH₂-CH=CH-C₆H₅

Figure 1: 1H-indole-2,3-dione derivatives (**P2** and **P3**)

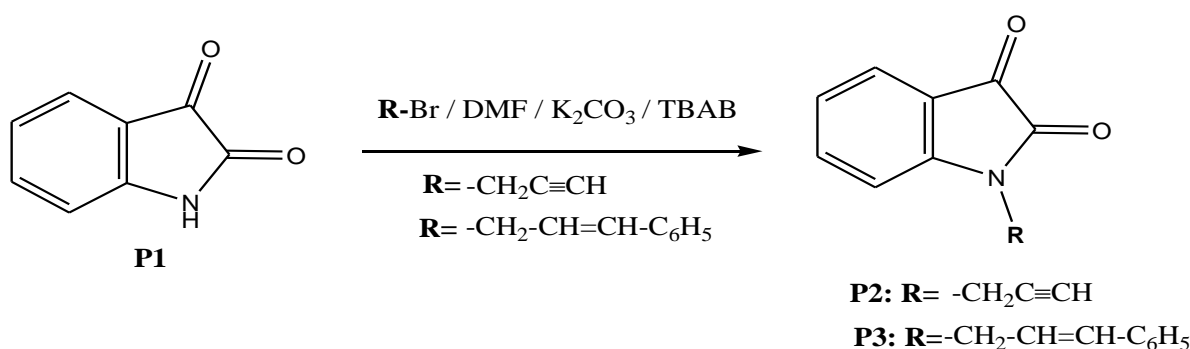
2. Experimental

2.1. Materials and solutions

The mild steel strips having a composition (wt.%) of 0.09% P, 0.01 % Al, 0.38 % Si, 0.05 % Mn, 0.21 % C, 0.05 % S and Fe balance were mechanically cut into 1.5 × 1.5 × 0.05 cm³ dimensions for the electrochemical experiments. The surface of the specimens was abraded with emery paper grade 600 and 1200, which was then washed in deionized water, degreased ultrasonically in ethanol and acetone. The acid solutions (1.0 M HCl) were prepared by dilution of analytical reagent-grade 98 % HCl with double-distilled water. The range of concentration of P2 was 10⁻⁶ M to 10⁻³ M.

2.2. Synthesis of inhibitor

To a solution of isatin (3.4 mmol) dissolved in DMF (30 ml) was added potassium carbonate (4.4 mmol), a catalytic quantity of tetra-n-butylammonium bromide (0.4 mmol) and 3-bromoprop-1-yne or 3-bromo-1-phenyl-1-propene (3.7 mmol). The mixture was stirred for 48 h; the reaction was monitored by thin layer chromatography. The mixture was filtered and the solvent removed under vacuum. The solid obtained was recrystallized from ethanol to afford the title compounds as red crystals (**P2**: yield 88%; m.p = 423K) and (**P3**: yield 86%; m.p = 413 K). (**Schema 1**):



Scheme 1: Synthesis of 1H-indole-2,3-dione (**P2** and **P3**).

The analytical and spectroscopic data are conforming to the structure of compounds formed:

(P2): Yield: 88%; **mp:** 423 K; **RMN¹H (DMSO-d₆) δ ppm:** 4.579 (d, 2H, CH₂, J=6.9 Hz); 2.32 (t, 1H, ≡CH, J=2.7 Hz); 7.152-7.699(m, 4H, CH_{arom}) **RMN¹³C (DMSO-d₆) δ ppm:** 149.62, 159.80(C=O) ; 117.71, 147.82(Cq) ; 111.08, 124.21, 125.50, 138.42(Carom) ; 75.66, (≡C-); 73.34(≡CH) ; 29.46(CH₂).

(P3): Yield: 86%; **mp:** 413 K; **RMN¹H (DMSO-d₆) δ ppm:** 4.781 (d, 2H, CH₂, J=6.9 Hz); 6.589 (d, 1H, C=CH_{arom}); 6.652 (m, 1H, CH=CH); 7.382-7.681(m, 9H, CH_{arom}); **RMN¹³C (DMSO-d₆) δ ppm:** 184.203, 159.124 (C=O); 147.128, 119.98, 139.52(Cq); 127.82, 127.981, 128.142, 129.5, 130.012, 124.58, 121.13, 120.573, 113.872 (Carom); 127.701, 133.891(CH=CH); 52.145(N-CH₂).

Mild steel corrosion behavior in 1 M HCl was investigated in the absence and presence of 1H-indole-2,3-dione derivatives (**P2** and **P3**) with the help of weight loss and electrochemical techniques. It was seen that mild steel dissolution rate was very high in 1 M HCl alone but the presence of inhibitor significantly decreased the corrosion rate of mild steel.

2.3. Electrochemical measurements

The electrochemical study was carried out using a potentiostat PGZ100 piloted by Voltmaster soft-ware. This potentiostat is connected to a cell with three electrode thermostats with double wall. A saturated calomel electrode (SCE) and platinum electrode were used as reference and auxiliary electrodes, respectively. Before all experiments, the potential was stabilized at free potential during 30 min. The solution test is there after de-aerated by bubbling nitrogen. The electrochemical impedance spectroscopy (EIS) measurements are carried out with the electrochemical system, which included a digital potentiostat model Voltalab PGZ100 computer at Ecorr after immersion in solution without bubbling. After the determination of steady-state current at a corrosion potential, sine wave voltage (10 mV) peak to peak, at frequencies between 100 kHz and 10 mHz are superimposed on the rest potential. Computer programs automatically controlled the measurements performed at rest potentials after 0.5 hour of exposure at 308 K. The impedance diagrams are given in the Nyquist representation. Experiments are repeated three times to ensure the reproducibility.

The inhibition efficiency of the inhibitor was calculated from the charge transfer resistance values using the following equation:

$$E_{R_{ct}} \% = \frac{R_{ct} - R_{ct}^{\circ}}{R_{ct}} \times 100 \quad (1)$$

Where, R_{ct}° and R_{ct} are the charge transfer resistance in absence and in presence of inhibitor, respectively.

2.4. Quantum chemical calculations

Quantum chemical calculations are used to correlate experimental data for inhibitors obtained from different techniques (viz., electrochemical and weight loss) and their structural and electronic properties. According to Koopman's theorem [7], E_{HOMO} and E_{LUMO} of the inhibitor molecule are related to the ionization potential (I) and the electron affinity (A), respectively. The ionization potential and the electron affinity are defined as $I = -E_{HOMO}$ and $A = -E_{LUMO}$, respectively. Then absolute electronegativity (χ) and global hardness (η) of the inhibitor molecule are approximated as follows [8]:

$$\chi = \frac{I+A}{2}, \quad \chi = -\frac{1}{2}(E_{HOMO} + E_{LUMO}) \quad (2)$$

$$\eta = \frac{I-A}{2}, \quad \eta = -\frac{1}{2}(E_{HOMO} - E_{LUMO}) \quad (3)$$

Where $I = -E_{HOMO}$ and $A = -E_{LUMO}$ are the ionization potential and electron affinity respectively.

The fraction of transferred electrons ΔN was calculated according to Pearson theory [9]. This parameter evaluates the electronic flow in a reaction of two systems with different electronegativities, in particular case; a metallic surface (Fe) and an inhibitor molecule. ΔN is given as follows:

$$\Delta N = \frac{\chi_{Fe} - \chi_{inh}}{2(\eta_{Fe} + \eta_{inh})} \quad (4)$$

Where χ_{Fe} and χ_{inh} denote the absolute electronegativity of an iron atom (Fe) and the inhibitor molecule, respectively; η_{Fe} and η_{inh} denote the absolute hardness of Fe atom and the inhibitor molecule, respectively. In order to apply the eq. 4 in the present study, a theoretical value for the electronegativity of bulk iron was used $\chi_{Fe} = 7$ eV and a global hardness of $\eta_{Fe} = 0$, by assuming that for a metallic bulk $I = A$ because they are softer than the neutral metallic atoms [9].

The electrophilicity has been introduced by Sastri *et al.* [10], is a descriptor of reactivity that allows a quantitative classification of the global electrophilic nature of a compound within a relative scale. They have proposed the ω as a measure of energy lowering owing to maximal electron flow between donor and acceptor and ω is defined as follows.

$$\omega = \frac{\chi^2}{2\eta} \quad (5)$$

The Softness σ is defined as the inverse of the η [11]

$$\sigma = \frac{1}{\eta} \quad (6)$$

Using left and right derivatives with respect to the number of electrons, electrophilic and nucleophilic Fukui functions for a site k in a molecule can be defined [12].

$$f_k^+ = P_k(N + 1) - P_k(N) \quad \text{for nucleophilic attack} \quad (7)$$

$$f_k^- = P_k(N) - P_k(N - 1) \quad \text{for electrophilic attack} \quad (8)$$

$$f_k^{\cdot} = [P_k(N + 1) - P_k(N - 1)]/2 \quad \text{for radical attack} \quad (9)$$

where, $P_k(N)$, $P_k(N+1)$ and $P_k(N-1)$ are the natural populations for the atom k in the neutral, anionic and cationic species respectively.

3. Results and discussion

3.1. Corrosion weight loss tests

The addition of 1H-indole-2,3-dione (P2 and P3), effect on mild steel corrosion in 1 M HCl solution was studied using weight loss measurement at 6 h of immersion. Table 1 represents the corrosion rate and the inhibition efficiency values. It is noted that P2 and P3 are good corrosion inhibitors for mild steel in acidic media. As the corrosion rate decreased, inhibition efficiency increased with increasing concentration and reached a maximum at 10^{-3} M of P3 and P2.

Table 1: Corrosion rate and inhibition efficiencies for mild steel in 1M HCl at various concentrations of P2 & P3

Inhibitor	Concentration (M)	ν (mg.cm ⁻² .h ⁻¹)	E_w (%)	θ
1M HCl	-	0.82	---	---
P2	10^{-6}	0.39	52	0.52
	10^{-5}	0.31	62	0.62
	10^{-4}	0.21	74	0.74
	10^{-3}	0.12	85	0.85
P3	10^{-6}	0.25	70	0.70
	10^{-5}	0.19	77	0.77
	10^{-4}	0.11	87	0.87
	10^{-3}	0.07	91	0.91

The presence of P3 gives high inhibiting efficiencies and P2 somewhat lower efficiency. This is probably due to the presence of phenyl ring in the P3 molecule. The organic compound containing the phenyl ring has better inhibition efficiency in acidic media compared to the organic compound without phenyl group.

3.2. Adsorption isotherm

The adsorption of 1H-indole-2,3-dione (P2 and P3) molecules at the metal solution interface minimizes the corrosion rate. This adsorption can be considered as a substitution adsorption process, where an organic compound from the aqueous media displaces the water molecules associated with the surface (H_2O_{ads}).



where 'x' is the number of water molecules replaced by the adsorption of 1H-indole-2,3-dione molecules. The mechanism of adsorption of organic molecules on the metal surface in the corrosive media can be established using surface coverage and inhibitor efficiency.

Using weight loss studies in the presence and absence of inhibitors, the surface coverage of the inhibitors was calculated using the relation:

$$\theta = E_w/100 \quad (11)$$

Various adsorption isotherms were tested and it was found that the adsorption of 1H-indole-2,3-dione (P2 and P3) molecules on the mild steel surface in acid medium followed Langmuir adsorption isotherm (Fig. 6), given by the expression:

$$\frac{C}{\theta} = \frac{1}{K} + C \quad (12)$$

Where, C is the concentration of inhibitor, K the adsorption equilibrium constant, and θ is the surface coverage.

The value of K_{ads} is determined from the plot of C_{inh} vs. C_{inh}/θ at constant temperature, which is used to calculate the value of the standard free energy of adsorption using the following expression:

$$\Delta G^{\circ}_{ads} = -RT \cdot \ln(55,5 \cdot K) \quad (13)$$

The plot obtained is linear with the correlation coefficient greater than 0.9. The negative values of ΔG_{ads} show the spontaneous adsorption of amisulpride molecules on the metal surface. Generally, the energy values of -20 kJ mol^{-1} or less negative are related with an electrostatic interaction between charged molecules and charged metal surface (physisorption); the values of -40 kJ mol^{-1} or more negative involve charge sharing or transfer between the inhibitor molecules to the metal surface to form a coordinate bond (chemisorption)[13,15]. The values of ΔG_{ads} for P2 and P3 are $-40.53 \text{ kJ mol}^{-1}$ and $-42.97 \text{ kJ mol}^{-1}$, respectively. Thus, in the present study, in HCl solution the 1H-indole-2,3-dione molecules get adsorbed on the metal surface by chemisorption [16]. The possible adsorption mechanism is direct adsorption on the basis of donor acceptor interactions between the lone pairs of electrons of heteroatoms, π -electrons of heterocyclic rings and the vacant d-orbitals of iron surface atoms. This process is called chemical adsorption.

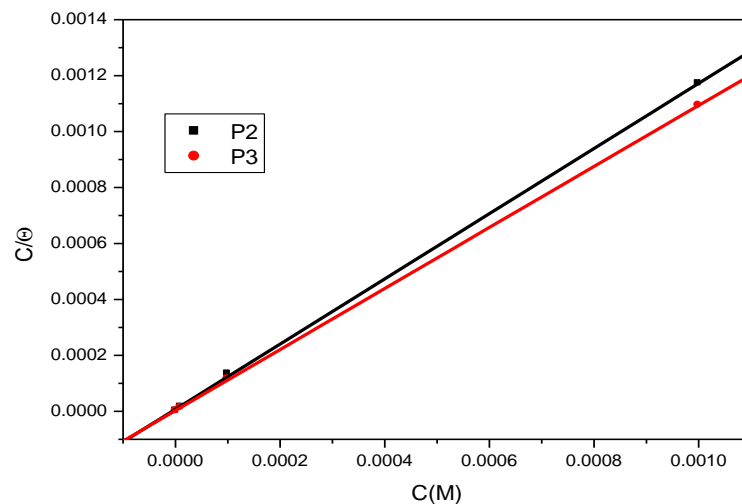


Figure 2: Langmuir isotherm adsorption model of each inhibitor on steel surface in 1.0 M HCl.

3.3. Tafel polarization studies

Figures 3 and 4 represent the cathodic and anodic Tafel plots for mild steel immersed in 1M HCl at 308 K in the absence and presence of different concentrations of P2 and P3. From figures 3, 4, it is clear that the polarization curves in 1.0 M HCl solutions with different concentrations of 1H-indole-2,3-dione derivatives are almost

similar: both anodic and cathodic reactions of mild steel electrode corrosion were inhibited, which suggested that these organic compounds reduce anodic dissolution and also retard the hydrogen evolution reaction. Cathodic Tafel curves give rise to parallel Tafel lines, indicating that the hydrogen evolution reaction is activation-controlled and the addition of the inhibitors does not affect the reduction mechanism, and their inhibition action is simply blocking the metal surface [17]. Electrochemical parameters such as corrosion potential (E_{corr}), cathodic Tafel slopes (β_c), corrosion current density (I_{corr}), and inhibition efficiency ($E_p\%$) are listed in Table 2.

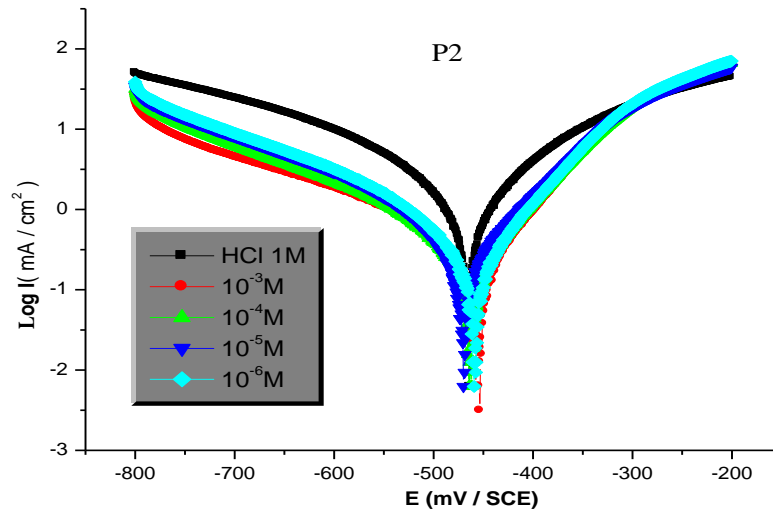


Figure 3: Potentiodynamic polarization curves for mild steel in 1 M HCl without and with different concentrations of P2 at 308 K.

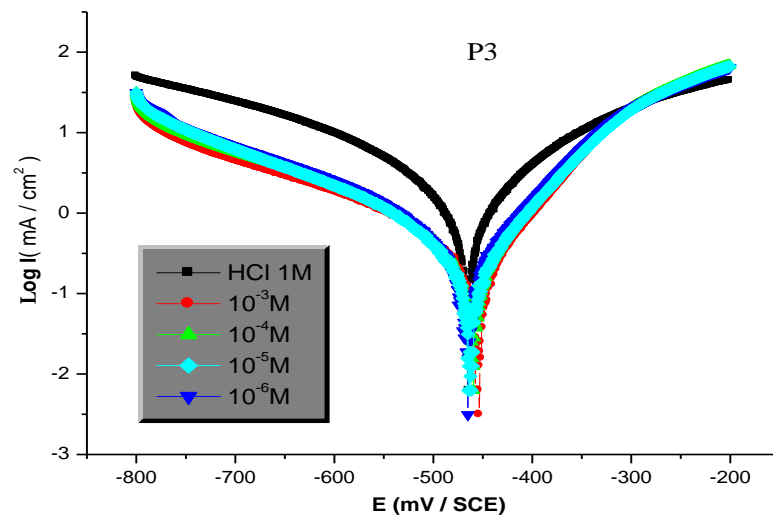


Figure 4: Potentiodynamic polarization curves for mild steel in 1 M HCl without and with different concentrations of P3 at 308 K.

Table 2 indicates that the values of corrosion current density in the inhibitor-containing solutions were lower than those for the blank acid solution. For all studied inhibitors, the corrosion current density decreases and the inhibition efficiency increases with increasing concentrations of inhibitors. P3 shows the maximum efficiency, 94% at a concentration of 10^{-3} M. There is no definite trend in the shift of E_{corr} values in the presence of various concentrations of inhibitors, suggesting that these compounds act as mixed-type inhibitors. It also shows that the cathodic Tafel slope (β_c) remains almost constant for P2. The constant β_c values indicate that the retardation of the cathodic reduction reaction is affected without changing the reaction mechanism. For P3, the cathodic Tafel

slope (β_c) shows a change with the addition of P3, which suggests that the inhibiting action occurred by simple blocking of the available cathodic sites on the metal surface, which led to a decrease in the exposed area necessary for hydrogen evolution and lowered the dissolution rate with increasing inhibitor concentration.

Table 2: Potentiodynamic polarization parameters for the corrosion of mild steel in 1 M HCl solution containing different concentrations of inhibitors P3 and P2 at 308K.

Inhibitor	Concentration (M)	$-E_{corr}$ (mV/SCE)	I_{corr} ($\mu\text{A}/\text{cm}^2$)	$-\beta_c$ (mV dec^{-1})	E_p (%)
1M HCl	-	464	1386	184	--
P2	10^{-6}	459	763	174	45
	10^{-5}	458	401	173	71
	10^{-4}	463	213	175	85
	10^{-3}	466	134	172	90
P3	10^{-6}	461	517	151	63
	10^{-5}	455	369	142	73
	10^{-4}	459	154	123	89
	10^{-3}	460	87	175	94

The efficiency order of inhibitors tested at all concentrations is as follows: P2 < P3. This order is the same as the one obtained from weight loss measurements and EIS measurements and also suggests that the differences in the inhibition efficiencies would be attributed to the differences in the structures among the four inhibitor molecules. Overall, the inhibition efficiencies obtained from Tafel polarization curves are higher than ones obtained from weight loss measurements, which is attributed to the different experimental conditions [18-19].

3.4. Electrochemical impedance spectroscopy

In order to improve the results extracted from gravimetric and polarization measurements and to acquire more information about corrosion mechanisms, Nyquist plots for mild steel after 0.5 h immersion in 1 M HCl solution in the absence and presence of different concentrations of P2 and P3 at 308K are given in Figures 5 and 6.

It is clear from this figures that all impedance spectra exhibit one single capacitive loop, which suggests that the corrosion of mild steel in 1 M HCl with and without inhibitors is mostly controlled by charge transfer process under the open circuit conditions, and usually related to the double layer behavior [20].

Moreover, these diagrams have a similar shape for all tested concentrations, indicating that there is quite no change in the corrosion mechanism [21]. In addition, these Nyquist plots are not perfect semicircles and this may be attributed to the frequency dispersion of interfacial impedance [22].

This behavior is a result of the surface roughness, the chemical heterogeneity of surface, and adsorption-desorption process of inhibitive molecules on mild steel surface [23]. Furthermore, the diameter of the semicircles in the presence of P2 and P3 is larger than observed in blank solution (1 M HCl) and increases with increasing inhibitors concentration, which may be related to the increase of surface coverage of inhibitive molecules on mild steel surface. Accordingly, the EIS data are simulated by the proposed equivalent circuit presented in Figure 5, where R_s is the solution resistance, R_{ct} denotes the charge-transfer resistance and CPE is constant phase element. The CPE element is used to explain the depression of the capacitance semi-circle, which corresponds to surface heterogeneity resulting from surface roughness, impurities, dislocations, grain boundaries, adsorption of inhibitors, formation of porous layers, etc. The impedance function of the CPE is represented by the expression [24, 29]:

$$Z_{CPE} = 1/Q(j\omega)^n \quad (14)$$

Where Q is the magnitude of the CPE, j is the imaginary number ($j^2 = -1$), ω is the angular frequency. a is the deviation parameter ($-1 \leq n \leq +1$), has the meaning of a phase shift. While $n = 0$, the CPE represents a pure resistor, for $n = -1$ an inductor and for $n = +1$, a pure capacitor [30]. In addition, the double layer capacitances, C_{dl} , for a circuit including a CPE were calculated by using the following equation [31]:

$$C_{dl} = Q(2\pi\omega_{max}) \quad (15)$$

Where $\omega_{max} = 2\pi f_{max}$ and f_{max} is the frequency at the maximum value of the imaginary part of the impedance spectrum.

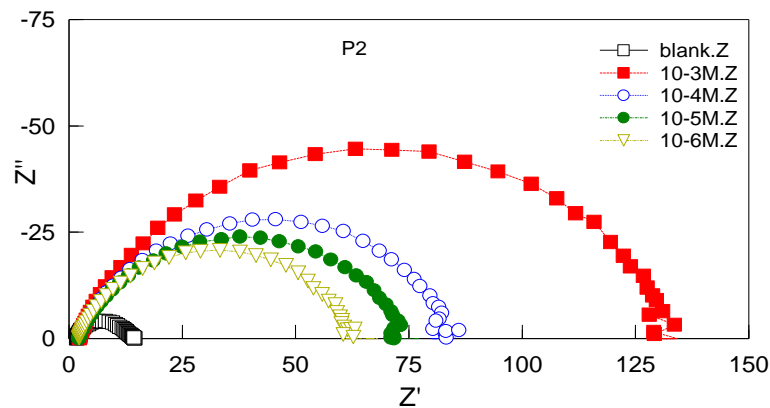


Figure 5: Nyquist impedance diagrams for mild steel obtained at 308k in 1 M HCl solution containing different concentrations of P2.

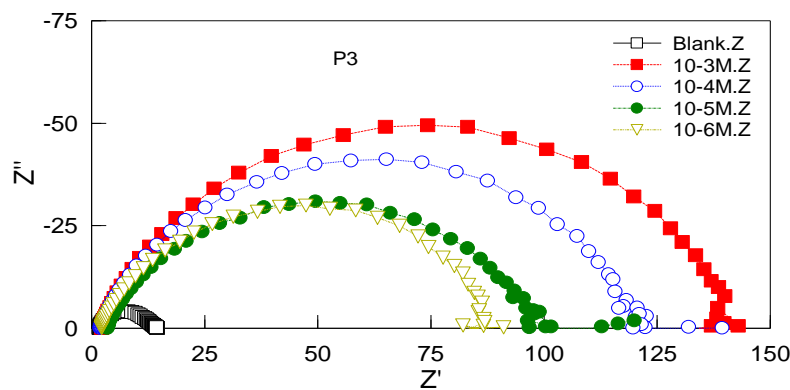


Figure 6: Nyquist impedance diagrams for mild steel obtained at 308k in 1 M HCl solution containing different concentrations of P3.

The corresponding Bode impedance magnitude and phase angle plots recorded for mild steel electrode immersed in 1 M HCl with and without different concentrations of inhibitors at its open potential circuit are given in Figures 7 and 8.

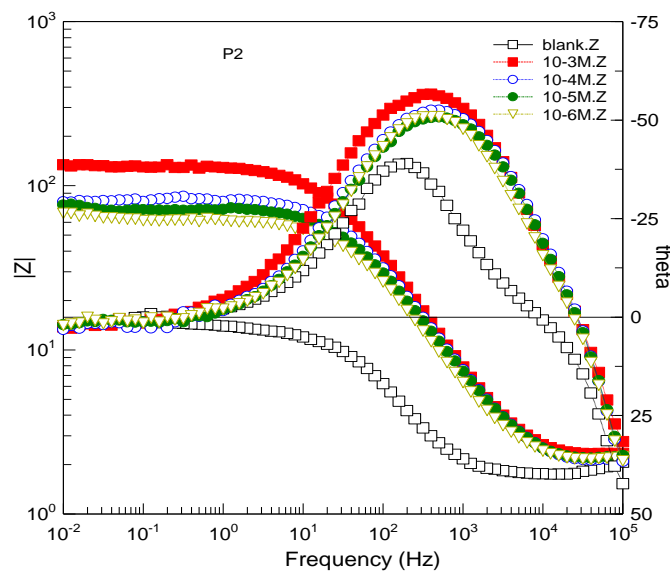


Figure 7: Bode and Phase angle plots of mild steel in 1 M HCl in the absence and presence of different concentrations of P2 at 308K.

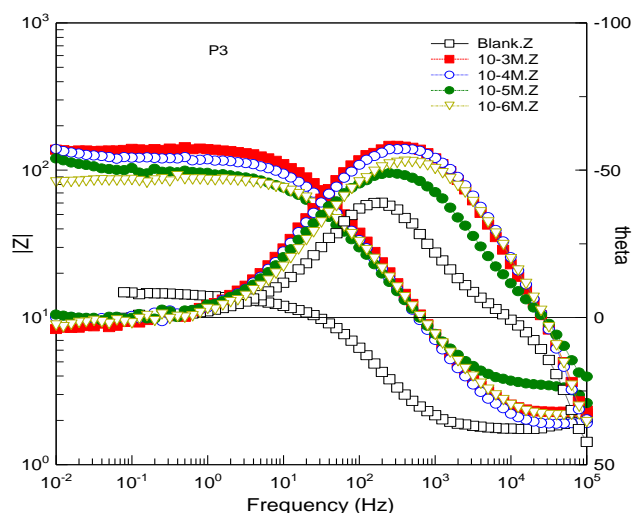


Figure 8: Bode and Phase angle plots of mild steel in 1 M HCl in the absence and presence of different concentrations of P3 at 308K.

As seen from Figure 7, Bode plots refer to the existence of an equivalent circuit containing a single constant phase element in the interface of metal/solution. The increase of absolute impedance at low frequencies in Bode plot confirms the higher protection with the increasing of inhibitors concentration [32]. According to appearance of phase angle plots, increasing the concentration of P2 and P3 inhibitors in 1 M HCl results in more negative values of phase angle indicating superior inhibitive behavior due to more inhibitor molecules adsorbed on mild steel surface at higher concentrations. As seen from Fig. 16, one phase peak at the center frequency range can be observed only, indicating that there is one time constant for P2 and P3, related to the electrical double layer [33]. The electrochemical parameters values such as R_s ($\Omega \text{ cm}^2$), R_{ct} ($\Omega \text{ cm}^2$), C_{dl} (IF cm_2) and E_{Rct} (%) of P2 and P3 were obtained from EIS and summarized in Table 3.

Table 3: EIS parameters for the corrosion of mild steel in 1 M HCl solution containing different concentrations of P3 and P2 at 308 K.

Inhibitor	Concentration (M)	R_{ct} ($\Omega \cdot \text{cm}^2$)	R_s ($\Omega \cdot \text{cm}^2$)	CPE ($\mu\Omega^{-1} \text{S}^n \text{cm}^{-2}$)	n	ω_{max} (Hz)	C_{dl} (μF)	E_{Rct} (%)
1M HCl	--	14.50	1.93	393	0.88	11	200	--
P2	10^{-6}	65	1.08	178	0.80	262	57	78
	10^{-5}	75	1.13	168	0.79	256	53	81
	10^{-4}	83	1.37	153	0.79	230	52	83
	10^{-3}	137	1.14	136	0.80	142	51	89
P3	10^{-6}	85	1.61	147	0.80	137	61	83
	10^{-5}	115	2.36	244	0.75	134	55	87
	10^{-4}	130	2.75	150	0.80	138	51	89
	10^{-3}	140	2.77	122	0.82	266	50	90

The C_{dl} values decrease while R_{ct} values increase with increasing inhibitors concentration. The highest R_{ct} ($137 \Omega \text{ cm}^2$ for P2 and $140 \Omega \text{ cm}^2$ for P3) have been found at optimum concentration (10^{-3} M). The increase in R_{ct} values is caused by adsorption of inhibitors, indicating that the exposed area decreased. On the other hand, a decrease in C_{dl} , which can result from a decrease in local dielectric constant and/or an increase in the thickness of the electrical double layer, suggests that P2 and P3 inhibitors act by adsorption at the metal–solution interface. Values of inhibition efficiency E_{Rct} increase with the concentration of these heterocyclic derivatives up to 89 % for P2 and 90% for P3, when concentration reaches 10^{-3} M . These results confirm once again that the title compounds exhibit efficient inhibitive performance for mild steel in hydrochloric acid solution and E_{Rct} follows the order: P3 > P2. It is worth noting that the inhibition efficiencies calculated from electrochemical measurements are reasonably in good agreement with those obtained from weight loss measurements as shown in Figure 9.

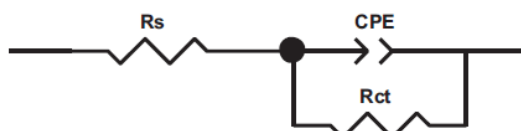


Figure 9: Equivalent circuits compatible with the experimental impedance data in Figure 10.

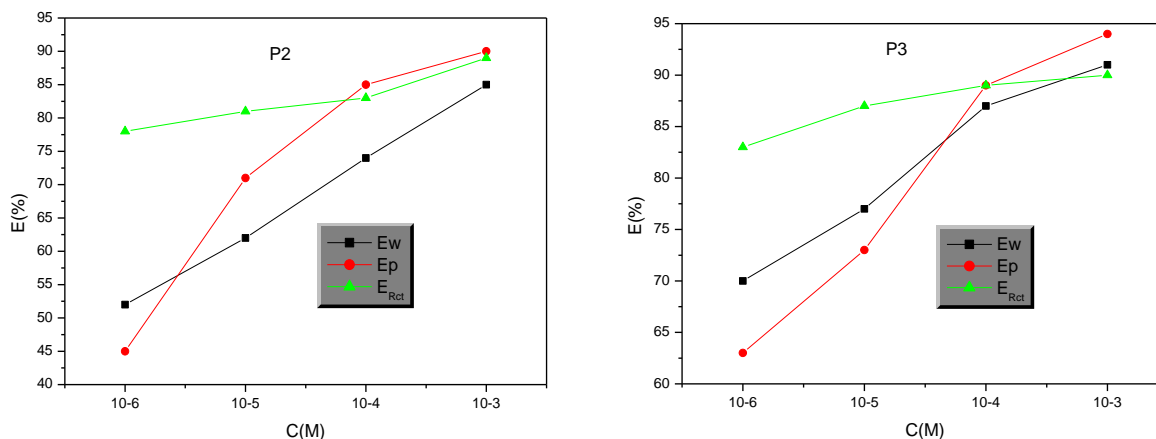


Figure 10: Variation of inhibition efficiency E (%) with inhibitor concentration at 308K measured by different methods.

3.5. Computational theoretical studies

The FMOs (HOMO and LUMO) are very important for describing chemical reactivity. The HOMO containing electrons, represents the ability (E_{HOMO}) to donate an electron, whereas, LUMO haven't not electrons, as an electron acceptor represents the ability (E_{LUMO}) to obtain an electron. The energy gap between HOMO and LUMO determines the kinetic stability, chemical reactivity, optical polarizability and chemical hardness–softness of a compound [34].

In this study, the HOMO and LUMO orbital energies were calculated using B3LYP method with 6-31G which is implemented in Gaussian 09 package [35]. All other calculations were performed using the results with some assumptions. The higher values of E_{HOMO} indicate an increase for the electron donor and this means a better inhibitory activity with increasing adsorption of the inhibitor on the metal surface, whereas the lower values of E_{LUMO} indicates the ability to accept electron of the molecule. The adsorption ability of the inhibitor to the metal surface increases with increasing of E_{HOMO} and decreasing of E_{LUMO} . The HOMO and LUMO orbital energies of the **P3** and **P4** inhibitors were performed and were given and shown in (Table 4) and (Figure 11), respectively. High ionization energy (> 6 eV) indicates high stability of **P3** and **P4** inhibitors [36]. The number of electrons transferred (ΔN), dipole moment, ionization potential, electron affinity, electronegativity, hardness, softness and total energy were also calculated and tabulated in (Table 4).

The nucleophilicity index (ω) is higher for the **P3** inhibitor than for **P2**, which indicates that **P3** is much more rich of electrons than **P2**. The energy gap ΔE is larger for **P2** than for **P3** providing therefore a low reactivity of the **P2**. The E_{HOMO} in aqueous phase is higher in the **P3** than in the **P2**, an indication that benzyl group increases the electron donating capacity of the **P3** inhibitor.

The value of ΔN (number of electrons transferred) show that the inhibition efficiency resulting from electron donation agrees with Lukovit's study [37]. If $\Delta N < 3.6$, the inhibition efficiency increases by increasing electron donation ability of these inhibitors to donate electrons to the metal surface [38]. The value of ΔN of **P3** (0.5279 and 0.5528 in gaseous and aqueous phases, respectively) is lighter than **P2** (0.4780 and 0.5006 in gaseous and aqueous phases, respectively), this indicates that **P3** is more electron donor compared to **P2**.

(Tables 5 and 6) display the most relevant values of the natural population ($P(N)$, $P(N-1)$ and $P(N+1)$) with the corresponding values of the Fukui functions (f_k^+ , f_k^- and f_k^0) of the studied inhibitors. The calculated values of the f_k^+ for **P2** and **P3** inhibitors are mostly localized on the isatine ring, namely C_5 , C_{13} , O_{14} , and O_{15} (**P2**) and C_5 , C_{13} , O_{14} , and O_{15} (**P3**), indicating that the isatine ring may be the most probable favorite site for nucleophilic attack.

Table 4: Quantum chemical parameters for **P2** and **P3** obtained in gaseous and aqueous phases using the DFT at the B3LYP/6-31G level.

Parameter	Gaseous Phase		Aqueous Phase	
	P2	P3	P2	P3
Total Energy TE (eV)	-17102.1	-23423.7	-17102.4	-23423.9
E_{HOMO} (eV)	-7.1492	-6.8156	-6.9957	-6.6534
E_{LUMO} (eV)	-0.0713	-0.1975	-0.1679	-0.0925
Gap ΔE (eV)	7.0779	6.6180	6.8278	6.5609
Dipole moment μ (Debye)	5.7800	6.4499	7.8224	8.4811
Ionization potential I (eV)	7.1492	6.8156	6.9957	6.6534
Electron affinity A	0.0713	0.1975	0.1679	0.0925
Electronegativity χ	3.6102	3.5066	3.5818	3.3730
Hardness η	3.5389	3.3090	3.4139	3.2804
Electrophilicity index ω	1.8415	1.8579	1.8790	1.7340
Softness σ	0.2826	0.3022	0.2929	0.3048
Fractions of electron transferred ΔN	0.4780	0.5279	0.5006	0.5528

Table 5: Pertinent natural populations and Fukui functions of **P2** calculated at B3LYP/6-31G in gaseous (G) and aqueous phases.

Atom k	Phase	$P(N)$	$P(N-1)$	$P(N+1)$	f_k^-	f_k^+	f_k^0
C₅	G	6,18557	6,29598	6,17019	0,1104	0,0154	0,0629
	A	6,17985	6,26528	6,17438	0,0854	0,0055	0,0454
C₁₃	G	5,51366	5,67873	5,53021	0,1651	-0,0166	0,0743
	A	5,49869	5,73207	5,50528	0,2334	-0,0066	0,1134
O₁₄	G	8,47708	8,63751	8,3872	0,1604	0,0899	0,1252
	A	8,52047	8,69173	8,44732	0,1713	0,0732	0,1222
O₁₅	G	8,54144	8,66215	8,40808	0,1207	0,1334	0,1270
	A	8,58051	8,69824	8,4585	0,1177	0,1220	0,1199

Table 6: Pertinent natural populations and Fukui functions of **P3** calculated at B3LYP/6-31G in gaseous (G) and aqueous phases.

Atom k	Phase	$P(N)$	$P(N-1)$	$P(N+1)$	f_k^-	f_k^+	f_k^0
C₅	G	6,187	6,28503	6,17936	0,0980	0,0076	0,0528
	A	6,18114	6,28441	6,17595	0,1033	0,0052	0,0542
C₁₃	G	5,52832	5,65788	5,52167	0,1296	0,0066	0,0681
	A	5,49898	5,69266	5,4991	0,1937	-0,0001	0,0968
O₁₄	G	8,47522	8,6245	8,40925	0,1493	0,0660	0,1076
	A	8,52396	8,69556	8,48349	0,1716	0,0405	0,1060
O₁₅	G	8,5167	8,6553	8,45993	0,1386	0,0568	0,0977
	A	8,58587	8,70199	8,52292	0,1161	0,0630	0,0895

The geometry of **P2** and **P3** in gaseous and aqueous phases (**Figure 11**) was fully optimized using DFT based on Beck's three parameters exchange functional and Lee–Yang–Parr nonlocal correlation functional (B3LYP)[38-39] and the 6–31G. The optimized molecular and selected angles, dihedral angles and bond lengths of **P2** and **P3** are given in (**Figure 11**). The optimized structure shows that the molecule **P2** and have a non-planar structure. The HOMO and LUMO electrons density distributions of **P2** and **P3** are given in (**Table 7**).

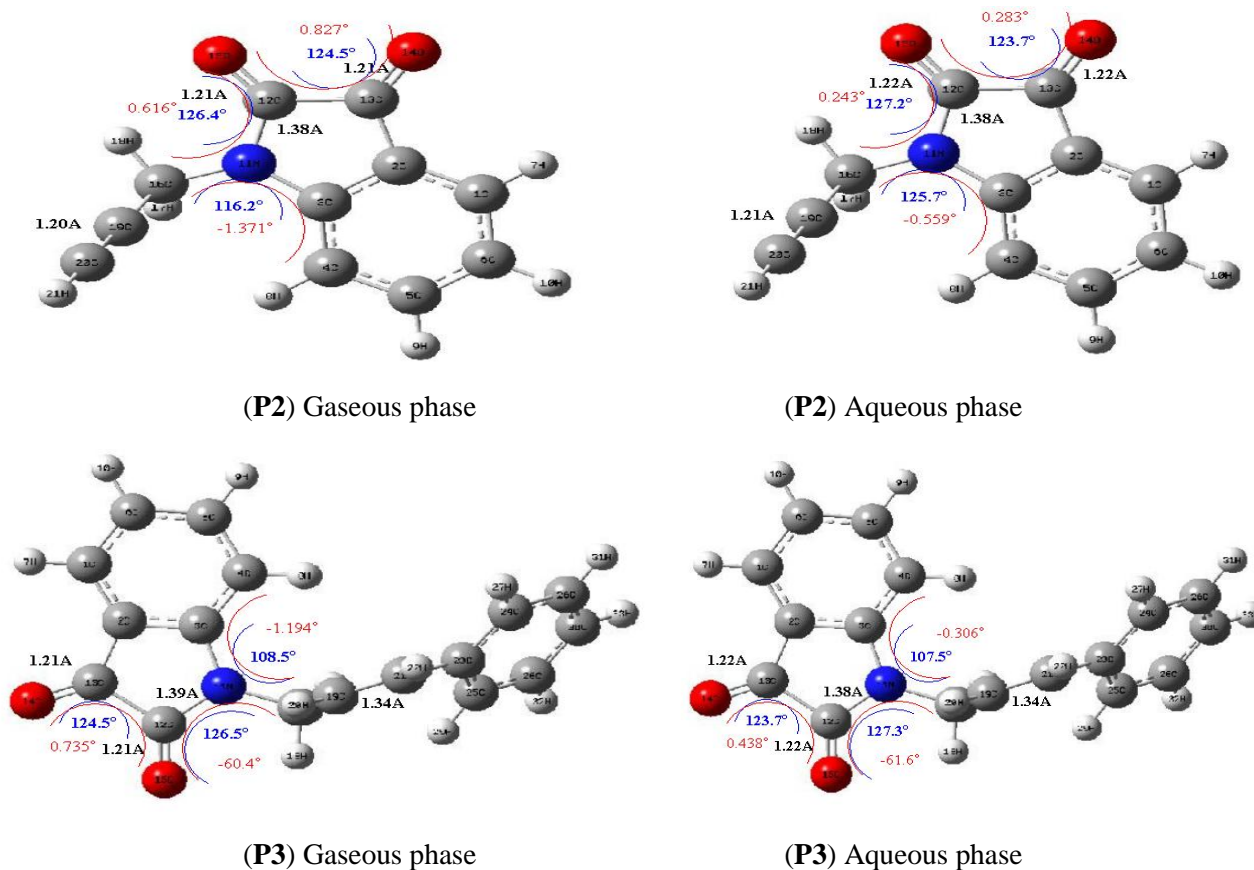
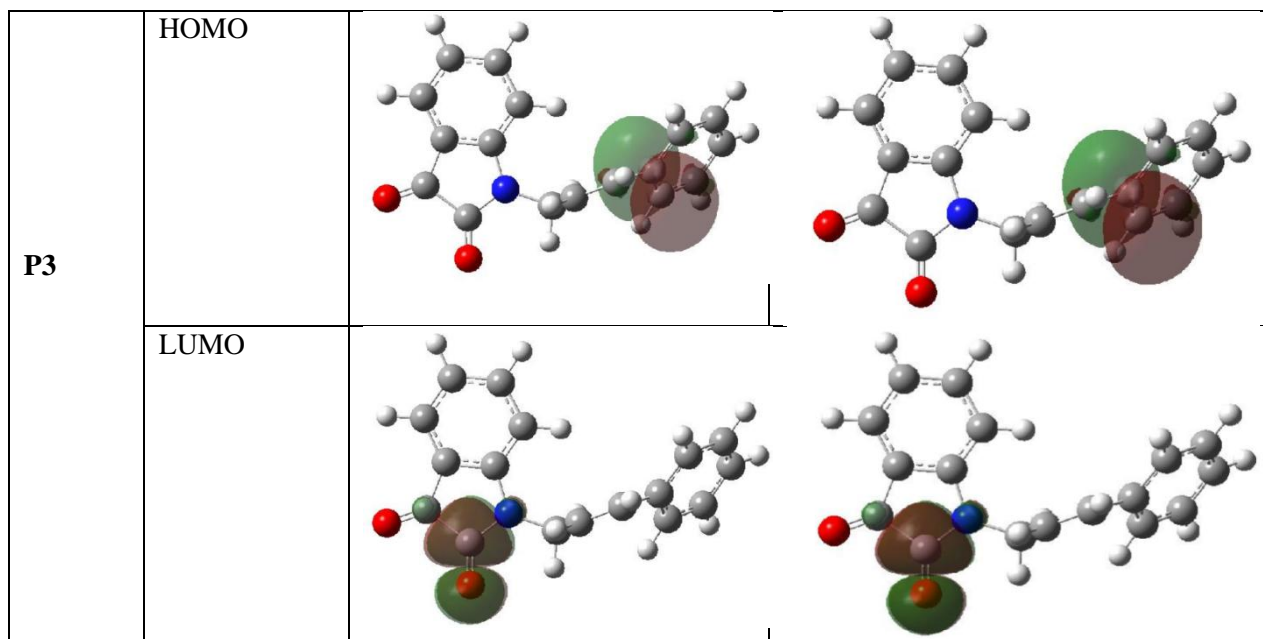


Figure 11: Optimized molecular structures and selected dihedral angles (red), angles (blue) and bond lengths (black) of the studied inhibitors calculated in gaseous and aqueous phases using the DFT at the B3LYP/6-31G level.

Table 7: The HOMO and the LUMO electrons density distributions of P2 and P3 in gaseous and aqueous phases computed at B3LYP/6-31G level for neutral forms.

Inhibitor	Type of MO	Gaseous Phase	Aqueous Phase
P2	HOMO		
	LUMO		



The large efficiency inhibition of **P3** with respect to **P2** is due to the presence of the benzyl group in **P3** inhibitor, which is electron-rich (π electrons), which increases the electron donor character of **P2**.

Conclusions

1H-indole-2,3-dione derivatives (**P2** and **P3**), have proved to be good inhibitors for the mild steel corrosion in 1 M HCl. These inhibitors act as mixed-type inhibitors. The inhibition efficiencies were found to increase with an increase in inhibitor concentrations. The electrochemical parameters obtained calculated from EIS show the same trend as those estimated from potentiodynamic polarization and weight loss measurements. The calculations of reactivity indices of **P2** and **P3** such as the localization of frontier molecular orbitals, E_{HOMO} , E_{LUMO} , energy gap (ΔE), dipole moment, hardness (η), softness (S), the fractions of electrons transferred (ΔN), electrophilicity index (ω), total energy change (TE), and natural bond orbital charge distributions together with local reactivity by means of Fukui indices put an accurate interpretation on the electron transfer mechanism between 1H-indole-2,3-dione molecules and the mild steel surface. Quantum chemical calculations substantiate the inhibition efficiencies obtained from experimental results.

Reference

- Pandeya S.N., Sriram D., *Acta Pharm. Tureica*.1 (1998) 33.
- Pandeya S.N., Yogeeshwari P., Sriram D., Nath G., *Indian J. Pharm. Sci.* 64(3) (2002) 209.
- Kiran G., Rajyalahshmi G., Rama Narsimha Reddy A., Venkateshwar R. J., Sarangapani M., *Journal. Res.* 2(3) (2009) 388.
- Selvam P., Muruges N., Chandramohan M., Debyser Z., Witvroum M., *Indian. J. Pharm. Sci.*70 (2008) 779.
- Singh G.S., Singh T., Lakhan R., *Indian. J.Chem.* 36B (1997) 951.
- Pramod K. S., Sakshi B., Divya M., Shashwat M., Brajendra K. S., Ashok K. P., Christophe L., Erik V. V .E., Balam G., Nigel G. J. R., Virinder S. P., *J. Enzyme. Inhib. Med. Chem.* (2016) 1475.
- Pearson R.G., *Inorg. Chem.* 27 (1988) 734.
- Sastri V.S., Perumareddi J.R., *Corrosion.* 53 (1997) 617.
- Elmsellem H., Nacer H., Halaimia F., Aouniti A., Lakehal I., Chetouani A., Al-Deyab S. S., Warad I., Touzani R., Hammouti B., *Int. J. Electrochem. Sci.* 9 (2014) 5328.
- Elmsellem H., Basbas N., Chetouani A., Aouniti A., Radi S., Messali M., Hammouti B., *Portugaliae. Electrochimica. Acta.* 2 (2014) 77.
- Udhayakala P., Rajendiran T. V., Gunasekaran S., *Chem. J.Biol. Phys. SCIA.* 2(3) (2012) 1151.
- Roy R.K., Pal S., Hirao K., *J. Chem. Phys.* 110 (1999) 8236.
- Sikine M., Kandri Rodi Y., Elmsellem H., Krim O., Steli H., Ouzidan Y., Kandri Rodi A., Ouazzani Chahdi F., Sebbar N. K., Essassi E. M., *J. Mater. Environ. Sci.* 7 (2016) 1386.

14. Hjouji M. Y., Djedid M., Elmsellem H., Kandri Rodi Y., Ouzidan Y., Ouazzani Chahdi F., Sebbar N. K., Essassi E. M., Abdel-Rahman I., Hammouti B., *J. Mater. Environ. Sci.* 7 (2016) 1425.
15. Qachchachi F. -Z., Kandri Rodi Y., Elmsellem H., Steli H., Haoudi A., Mazzah A., Ouzidan Y., Sebbar N. K., Essassi E. M., *J. Mater. Environ. Sci.* 7 (8) (2016) 2897.
16. Elmsellem H., Aouniti A., Youssofi M.H., Bendaha H., Ben hadda T., Chetouani A., Warad I., Hammouti B., *Phys. Chem. News.* 70 (2013) 84.
17. Filali Baba Y., Elmsellem H., Kandri Rodi Y., Steli H., AD C., Ouzidan Y., Ouazzani Chahdi F., Sebbar N. K., Essassi E. M., Hammouti B., *Der Pharma Chemica*, 8 (2016) 159.
18. Elmsellem H., Karrouchi K., Aouniti A., Hammouti B., Radi S., Taoufik J., Ansar M., Dahmani M., Steli H., El Mahi B., *Der Pharma Chemica* 7 (2015) 237.
19. Qachchachi F. Z., Kandri Rodi Y., Essassi E. M., Bodensteiner M., El Ammari L., *Acta Cryst.* E70 (2014) o588.
20. Xu B., Yang W., Liu Y., Yin X., Gong W., Chen Y., *Corros. Sci.* 78 (2014) 260.
21. Elmsellem H., Aouniti A., Youssofi M.H., Bendaha H., Ben hadda T., Chetouani A., Warad I., Hammouti B., *Phys. Chem. News.* 70 (2013) 84.
22. Li X., Xie X., Deng S., Du G., *Corros. Sci.* 87 (2014) 27.
23. Elmsellem H., Harit T., Aouniti A., Malek F., Riahi A., Chetouani A., Hammouti B., *Protection of Metals and Physical. Chemistry of Surfaces.* 5 (2015) 873.
24. Chakib I., Elmsellem H., Sebbar N. K., Lahmidi S., Nadeem A., Essassi E. M., Ouzidan Y., Abdel-Rahman I., Bentiss F., Hammouti B., *J. Mater. Environ. Sci.* 7 (2016) 1866.
25. Zhang Q.B., Hua Y.X., *Electrochim. Acta.* 54 (2009) 1881.
26. Elmsellem H., Aouniti A., Toubi Y., Steli H., Elazzouzi M., Radi S., Elmahi B., El Ouadi Y., Chetouani A., Hammouti B., *Der Pharma Chemica*, 7(7) (2015) 353.
27. Labjar N., Lebrini M., Bentiss F., Chihib N.E., El Hajjaji S., Jama C., *Mater. Chem. Phys.* 119 (2010) 330.
28. Elmsellem H., Elyoussfi A., Steli H., Sebbar N. K., Essassi E. M., Dahmani M., El Ouadi Y., Aouniti A., El Mahi B., Hammouti B., *Der Pharma Chemica.* 8(1) (2016) 248.
29. Ehteshamzadeh M., Jafari A.H., Naderi E., Hosseini M.G., *Mater. Chem. Phys.* 113 (2009) 986.
30. Elmsellem H., Elyoussfi A., Sebbar N. K., Dafali A., Cherrak K., Steli H., Essassi E. M., Aouniti A. and Hammouti B., *Maghr. J. Pure & Appl. Sci.* 1 (2015) 1.
31. Hosseini M., Mertens S.F.L., Ghorbani M., Arshadi M.R., *Mater. Chem. Phys.* 78 (2003) 800.
32. Elmsellem H., Aouniti A., Khoutoul M., Chetouani A., Hammouti B., Benchat N., Touzani R. and Elazzouzi M., *J. Chem. Pharm. Res.* 6 (2014) 1216.
33. Sikine M., Kandri Rodi Y., Elmsellem H., Krim O., Steli H., Ouzidan Y., Kandri Rodi A., Ouazzani Chahdi F., Sebbar N. K., Essassi E. M., *J. Mater. Environ. Sci.* 7 (2016) 1386.
34. Govindarajan M., Karabacak M., *Spectrochim. Acta Part A Mol. Biomol. Spectrosc.* 85 (2012) 251.
35. Becke A.D., *J. Chem. Phys.* 98 (1993) 1372.
36. Hjouji M. Y., Djedid M., Elmsellem H., Kandri Rodi Y., Benalia M., Steli H., Ouzidan Y., Ouazzani Chahdi F., Essassi E. M., Hammouti B., *Der Pharma Chemica.* 8(4) (2016) 85.
37. Lukovits I., Kalman E., Zucchi F., *Corrosion.* 57 (2001) 3.
38. Elmsellem H., Elyoussfi A., Steli H., Sebbar N. K., Essassi E. M., Dahmani M., El Ouadi Y., Aouniti A., El Mahi B., Hammouti B., *Der Pharma Chemica.* 8(1) (2016) 248.
39. Lee C., Yang W., Parr R.G., *Phys. Rev. B.* 37 (1988) 785.

(2016) ; <http://www.jmaterenvirosci.com/>